Excited-State Coordination Chemistry: Excited-State Basicity of Bis(2,2′-bipyridyl)(2,3-dipyridylpyrazine)ruthenium(II)

José L. Zambrana, Jr., Elena X. Ferloni, and Harry D. Gafney*

Department of Chemistry & Biochemistry, Queens College of the City University of New York

Received: April 16, 2009; Revised Manuscript Received: September 8, 2009

The proton dependencies of the absorption and emission spectra of bis(2,2′-bipyridyl)(2,3-bis(2-pyridyl)pyrazine)ruthenium(II), $(bpy)_2Ru(dpp)^{2+}$ indicate that population of the dpp-localized MLCT state increases the basicity of dpp peripheral nitrogens. NMR spectra reveal the protonation of the peripheral dpp pyridine in the ground state, pK_a of 1.12 ± 0.03, occurs intermediate between the changes evident in the absorption and emission spectra. As a result, the emissivity of aqueous solutions of $(bpy)_2Ru(dpp)^{2+}$ as a function of $[H^+]$ derives from two emissive species: the unprotonated complex and the monoprotonated complex $[(bpy)_2Ru(dppH_{py})]^{3+}$ with the proton attached to the peripheral dpp pyridine. Although protonation in the MLCT state generally quenches the emission, the emissivity of the monoprotonated complex, albeit weak, is attributed to the asymmetric distribution of the charge in the MLCT state. The majority of the transferred charge resides at the peripheral pyrazinyl nitrogen, and excited-state acid−base chemistry occurs predominantly at this site. Nonetheless, ground-state protonation of the peripheral dpp pyridine dramatically increases the nonradiative decay rate and significantly influences subsequent excited-state protonation processes. Protonation of the excited state changes from a bimolecular process to a combination of inter- and intramolecular processes where the proton transfers from the dpp pyridyl nitrogen to the dpp pyrazinyl nitrogen and from the surrounding aqueous solvent shell. Energetically, changes in the absorption spectra originally attributed to the first protonation of the complex and from which the ΔpK_a of the excited state have been estimated, in fact, correspond to the second protonation of the complex.

Introduction

The hydrogen ion dependencies of the absorption and emission spectra of Ru(II) diimines reveal substantial differences in the acid−base properties of the ground and emissive MLCT states of the complexes.[1] Depending on the direction of the charge transfer relative to the acid−base site, and the location of the acceptor orbital in the MLCT state, excitation changes electron distribution, which in turn increases or decreases acid−base properties by as much as 5 to 6 orders of magnitude.[2] Brønsted basicity usually does not correlate with the coordinating ability of a ligand, but, with diimine ligands, the equilibrium constant for coordination increases linearly with the Brønsted basicity of the ligand's coordinating nitrogens.[3] Work in this laboratory focuses on whether these photoinduced changes in acid−base properties translate into an excited-state coordination chemistry where a Ru(II) diimine possessing one or more acid−base sites on the ligand periphery functions as a ligand and whether excitation enhances or reduces its ability to coordinate to another metal.

Excited-state coordination chemistry arises from the observation that excitation of bis(2,2′-bipyridyl)(2,3-dipyridylpyrazine)ruthenium(II), $(bpy)_2Ru(dpp)^{2+}$, in the presence of $PtCl_6^{2-}$ leads to the formation of the bimetallic $[bpy)_2Ru(dpp)PtCl_4]^{2+}$.[4] The absence of an equivalent chemistry with metal ions that form stable diimine complexes and quench by electron or energy transfer mechanisms led to the proposal that $[(bpy)_2Ru(dpp)PtCl_4]^{2+}$ formation occurs via an excited-state coordination chemistry rather than the more familiar electron or energy transfer mechanisms. With a chelation site on the dpp periphery structurally analogous to that in bpy, $(bpy)_2Ru(dpp)^{2+}$ is viewed as a ligand, and the increased basicity induced by excitation is thought to increase the equilibrium constant for coordination to the Pt(IV), thereby enhancing bimetallic formation. Unlike $(bpy)_2Ru(dpp)^{2+}$, where the population of the emissive MLCT state increases electron density at the peripheral dpp nitrogens, population of the MLCT state in *cis*-$(bpy)_2Ru(CN)_2$ shifts electron density to the bpy ligands, which inductively reduces electron density at the cyano groups and reduces their basicity by ca. 5 orders of magnitude.[5] The $[H^+]$ dependence of the quantum yield of dissociation of the bimetallic $[bpy)_2Ru(CN)(\mu\text{-}CN)Rh(NH_3)_4Br]^{2+}$ and the appearance of a $(bpy)_2Ru(CN)_2$ emission from a bimetallic composed of two components that, as individual molecules quench at a diffusion controlled rate, led to the suggestion that optical excitation of the $(bpy)_2Ru(CN)_2$ ligand in $[bpy)_2Ru(CN)(\mu\text{-}CN)Rh(NH_3)_4Br]^{2+}$ leads to a dissociative excited state.[6] Dissociation is attributed to the reduction in electron density at the cyano groups as evidenced by the decrease in their basicity on the population of the $(bpy)_2Ru(CN)_2$ ligand's MLCT state.

Excited-state coordination is thought to arise from the photoinduced changes in acid−base properties evident in the hydrogen ion dependencies of the complexes' absorption and emission spectra. All excited state pK_a measurements are subject to the uncertainty of whether the excited state achieves equilibrium under a given set of experimental conditions and therefore whether changes derived from the spectral changes reflect the actual or usable changes in acid−base properties. An additional complication exists in systems containing two or more basic sites in close proximity, which is the situation encountered when the site is also capable of functioning as a

* To whom correspondence should be addressed. E-mail: Harry.Gafney@qc.cuny.edu.

10.1021/jp903521p CCC: $40.75
Published on Web 10/22/2009

chelate. As pointed out by Shimidzu and co-workers,[7] the relative basicities of different sites in the excited state may not be equivalent to that in the ground state. In which case, the ΔpK_a calculated from the $[H^+]$ dependence of the absorption and emission measures a general change in acid−base properties but does not necessarily follow the change in acid−base properties of a specific site or specific donor atom. The basic sites in $(bpy)_2Ru(dpp)^{2+}$ that function as the chelation site for other metal ions are the pyrazinyl and pyridyl nitrogens on the dpp periphery. The inductive effect of the cationic metal reduces the electron density at the pyrazinyl nitrogen para to Ru(II), thereby reducing its basicity.[8]

In the ground state, pyridines are generally more basic than pyrazine with protonation usually occurring in the 1 to 3 pH range. However, absorption spectra of $(bpy)_2Ru(dpp)^{2+}$ recorded as a function of $[H^+]$ fail to exhibit any significant changes in the MLCT absorptions in the 1 to 3 pH range[9] that would suggest protonation of the dpp peripheral pyridine. The only significant change occurs at high acidity, in the −3 to −5 range on the Hammett acidity scale, where the $(bpy)_2Ru(dpp)^{2+}$ MLCT absorptions at 430 and 470 nm are replaced by an absorption with a maximum at 573 nm.[8] Given the presence of an isosbestic point, these spectral changes, which are quantitatively reversible on the addition of a base, are assigned to the first protonation of the complex, although the specific dpp peripheral nitrogen protonated has yet to be identified.

The $(bpy)_2Ru(dpp)^{2+}$ emission intensity declines as the pH decreases from 5 to 3. Plots of the relative intensity versus pH exhibit a single inflection point corresponding to a pK_a^* of 2.8. Nazeeruddin and Kalyanasundaram[9] assign these spectral changes to protonation of the MLCT state and, relative to the ground-state pK_a of −3.8 obtained from the changes in the MLCT absorptions, calculate the ΔpK_a to be 6.6. However, Strekas and co-workers point out that, the peripheral pyridyl nitrogen of dpp, which is out of the plane of the pyrazine and the other pyridine ring coordinated to Ru(II), is not as strongly coupled electronically and therefore less susceptible to the inductive effect of Ru(II).[8] Consequently, the basicity of this site in the ground state would be expected to be similar to the basicity of pyridine itself. Although there is no significant change in the $(bpy)_2Ru(dpp)^{2+}$ absorption spectrum suggestive of protonation in the 1 to 3 pH range, a protonation step in this pH range is particularly relevant to excited-state coordination chemistry because the measured ΔpK_a, the difference between pH dependent changes in the emission spectra relative to that observed in the absorption spectra, would be smaller. Assuming excited-state coordination of $(bpy)_2Ru(dpp)^{2+}$ parallels that of ground-state diimines, that is the equilibrium constant for coordination increases linearly with the basicity of the coordinating nitrogens; the extent of coordination induced by excitation will be smaller than that expected based on $\Delta pK_a = 6.6$.

The detection of previously unreported emissions from $(bpy)_2Ru(dpp)^{2+}$ spurred these experiments to identify the sequence of protonations of the peripheral dpp nitrogens in the ground and excited states. With two potential protonation sites, an immediate question is whether emission and absorption monitor protonation at an equivalent site? NMR spectra specify the first protonation of $(bpy)_2Ru(dpp)^{2+}$ at the pyridyl nitrogen in the pH 0−2 range, which is followed by the second protonation at the pyrazinyl nitrogen at much higher acidity. Thus, with multiple protonation sites with different pK_a's, calculation of excited-state pK_a's must be approached with caution, as each site must be evaluated individually. The change in basicity then calculated at each site has implications for how the excited-state might be used to achieve coordination to metals. Moreover, the additional detection and analysis of previously unreported emissions from $(bpy)_2Ru(dppH)^{3+}$ suggest two things: first, because the peripheral pyridine is minimally electronically coupled to the remainder of the ligand or the complex, the monoprotonated complex with the proton at the pyridyl nitrogen remains weakly emissive; second, whereas the excited-state $(bpy)_2Ru(dpp)^{2+}$ is quenched by protonation at the pyrazinyl nitrogen, proton quenching of $(bpy)_2Ru(dppH)^{3+}$ may in fact occur by intramolecular transfer of the proton from the pyridyl nitrogen to the pyrazinyl nitrogen, which renders the complex nonemissive.

Experimental Methods

Materials. $Ru(bpy)_2(dpp)^{2+}$ was prepared and purified as previously described[10] but precipitated as $[Ru(bpy)_2(dpp)](PF_6)_2$. Absorption and emission spectra of the complex and its emission lifetime in room temperature aqueous solution agreed with published data.[10] To achieve the concentration needed to carry out the NMR experiments, the hexafluorophosphate salt was converted to the nitrate form, $[Ru(bpy)_2(dpp)](NO_3)_2$, by charging the complex onto a Dowex 1-X8 strongly basic anion-exchange resin (Fluka, Lot 427365/1) and eluting with a saturated solution of $NaNO_3$. The eluent was evaporated to dryness, dissolved in a minimum of acetonitrile, and the complex was purified using an alumina column and eluting with acetonitrile. At wavelengths ≥350 nm, absorption and emission spectra of the nitrate salt are identical to those of PF_6^- and ClO_4^- salts,[8] and, within an experimental uncertainty of 10%, the emission lifetime of the complex in room temperature, aqueous solution is independent of the counteranion.

D_2O with 0.1% v/v DSS (Sigma-Aldrich, Lot 67231KU, 99.9%) and D_2SO_4 (Sigma Aldrich, 99.9%) were used as received. The pH of aqueous solutions was adjusted using standard buffer solutions. The pD of D_2O solutions were adjusted by the addition of standardized D_2SO_4.

Physical Measurements. Absorption spectra were recorded either on an Aviv Model 1400 or PerkinElmer Lambda 3 spectrophotometer. Steady-state excitation was achieved with 488 nm light from a Coherent Innova Argon Ion laser and pulsed excitation used 532 nm light (8 ns fwhm) from a Nd:YAG laser. All spectra were recorded on a Princeton Instruments PI-MAX Gen II red sensitive ICCD camera coupled to an Acton SP300i Spectrograph (grating blazed for sensitivity at 800 nm, 500 grooves/mm). The wavelength scale of the spectrograph-ICCD camera was calibrated with an AnaLamp Hg pen lamp (BHK Corporation, Model #81−1057−01). For emission decay measurements, sequencing the laser pulse and camera scan was accomplished with a Stanford DG-535 Timing Generator. To compensate for an 85 ns delay in triggering the camera; however, resistance was added to the external trigger circuit of the laser to delay the laser pulse by the appropriate time. All decays were tested against single and double exponentials to determine the best fit. In all cases, fits obtained with a single exponential were equal to those obtained with a double exponential. Consequently, the lifetimes reported here are extracted from the single exponential fits. Picosecond excitation of room temperature, acidic aqueous solutions of the complex was accomplished with the 400 nm, second harmonic of a Coherent Mira Modelocked Ti:Sapphire laser. Light emitted in the 450 to 750 nm region was isolated by means of glass filters, and its time dependence was determined with a Hammamatsu, Model C1587 streak camera.

Emission spectra of $Ru(bpy)_2(dpp)^{2+}$ recorded with the spectrograph-ICCD camera exhibited maxima red-shifted from previously recorded spectra under equivalent conditions. For example, the emission maximum from room temperature, 22 ± 1 °C, aqueous solutions of $Ru(bpy)_2(dpp)^{2+}$, originally reported to occur at 675 nm,[10] appeared at 705 nm in spectra recorded with the spectrograph-ICCD camera. The argon lines available from the Hg pen lamp revealed that the ICCD camera exhibits a higher sensitivity in the red than previously used detectors. Because the emission maximum is independent of the counterion of the complex, that is whether $[Ru(bpy)_2(dpp)](PF_6)_2$ or $[Ru(bpy)_2(dpp)](NO_3)_2$ was used, and the emission lifetime measured at 705 nm, 126 ± 7 ns is within experimental error of the previously reported value, 135 ± 14 ns,[10] the difference in the emission maxima is attributed to higher sensitivity of the spectrograph-ICCD camera at longer wavelengths.

Emission quantum yields were determined by the gradient method to minimize error.[11] The areas of the emission spectra obtained with steady-state excitation, proportional to quantum yield of emission, were plotted at various absorbance values (OD < 0.1) for the reference and the complex in question. The ratio of their linear slopes, or gradients, is equivalent to the ratio of their emission quantum yields. Because of the exceptional sensitivity of the ICCD at longer wavelengths, uncorrected spectra were used. The quantum yield of emission from room temperature, 22 ± 1 °C, deaerated (N_2 or Ar bubbling), solutions of $Ru(bpy)_2(dpp)^{2+}$ in pH 7 standard buffer was measured relative to an aqueous solution of $Ru(bpy)_3^{2+}$, which was excited with 488 nm light from an Ar^+ laser, and the emission spectra recorded with the spectrograph-ICCD camera.

The major difficulty in measuring the quantum efficiency of emission from the protonated complex is the huge difference in its emissivity relative to that of a standard, such as $Os(bpy)_3^{2+}$, or the unprotonated complex. The difference is so large, $\geq 10^3$, it is not possible to measure the intensities from the protonated complex and the standard with the same emission spectrometer settings. Consequently, the quantum yield of the 735 nm emission from the protonated complex was measured relative to the 705 nm emission from the unprotonated complex utilizing the ICCD camera gain to compensate for the differences in intensities and using solutions of much higher OD (<1). The unprotonated complex was chosen as a standard because its emission spectrum overlaps part of that of the protonated complex, and the absorption spectra of the protonated and unprotonated complexes are extremely similar within the relevant pH range. Two solutions containing the same amount of $Ru(bpy)_2(dpp)^{2+}$, ca. 10^{-4} M, were prepared. One was made 0.1 M in HNO_3 whereas the other was buffered to pH 7. A calibration plot of the area under the 705 nm emission curve versus camera gain was constructed (Figure 1), and the data fit to the expected exponential dependence on camera gain.[12]

The ratio of the areas of the 705 nm emission at the different gains was then used to calculate the quantum yield of the protonated complex from the ratio of its gradient to that of the unprotonated complex. High concentrations of the complex and high, 488 nm excitation intensities are necessary to maximize the intensity of the 735 nm emission, but spectra recorded before and after the measurements gave no indication of degradation of the complex and its monoprotonated analogue. Nonetheless, a collective uncertainty of ca. 20% is estimated in the reported value of the quantum yield of emission for the protonated complex, Φ_{em}^{P}.

NMR spectra were recorded with a Bruker DPX 400 MHz FT-NMR operating at 400.13 MHz, with 16 scans, 8300 Hz spectral width, 2s acquisition time, and a 6.00 μs 90° flip angle. All experiments were carried out in 99.9% D_2O and referenced to DSS. Two-parameter curve-fitting of the changes in chemical shift data was accomplished by nonlinear regression using Microsoft Excel's solver.

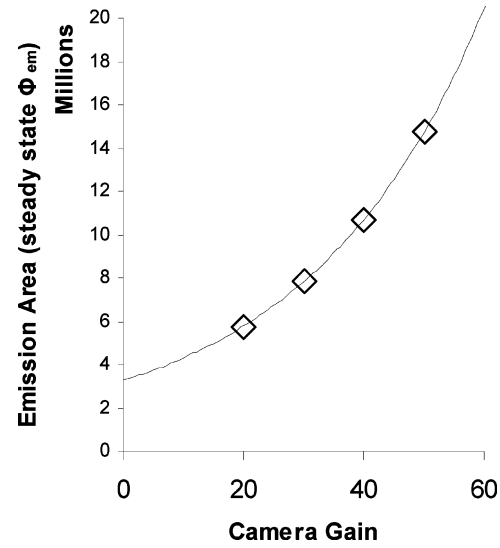

Figure 1. Plot of the area of the 705 nm emission from $Ru(bpy)_2(dpp)^{2+}$ (◊) vs ICCD camera gain. Solid line shows the fit of the data obtained with the exponential function used to calculate the ratios of the 705 nm emission areas at the different gains.

Results

I. Absorption Spectroscopy. $Ru(bpy)_2(dpp)^{2+}$ exhibits two MLCT transitions at 23 400 cm^{-1} (428 nm, $\varepsilon = 9.7 \times 10^3$ $M^{-1}\cdot cm^{-1}$), which is the charge transfer to bpy, and at 21 000 cm^{-1} (476 nm, $\varepsilon = 9.2 \times 10^3$ $M^{-1}\cdot cm^{-1}$), which is the charge transfer to dpp. The intense UV absorptions ($\lambda < 350$ nm) exhibit some dependence on pH, but the changes are small and being among a number of intense absorptions were not pursued experimentally. Consistent with previous studies, only slight changes in the MLCT absorption maxima occur in the pH 7 to 0 range; the bpy localized, 23 400 cm^{-1} (428 nm) MLCT transition shifts to 23 700 cm^{-1} (422 nm) and increases in intensity by 17%, whereas the dpp localized, 21 000 cm^{-1} (476 nm) MLCT shifts from 600 to 20400 cm^{-1} (490 nm) and decreases in intensity by 10%. When the solution becomes highly acidic, however, corresponding to Hammett acidity (H_o) values of −4 to −6, the solution changes from the characteristic Ru(II) diimine reddish-orange to purple. The 23 700 cm^{-1} (422 nm) and 20 400 cm^{-1} (490 nm) MLCT absorbances are replaced by a band with a maximum at 17 500 cm^{-1} (573 nm) skewed to shorter wavelengths with a shoulder in the 26 300 cm^{-1} (380 nm) region. Adding NaOH reverses the spectral changes, and the system can be cycled quantitatively between the protonated and unprotonated complexes at least three times. Quantitative reversibility places the molar extinction coefficient for the diprotonated species at 17 500 cm^{-1} (573 nm) to be 1.8×10^3 $L\cdot mol^{-1}\cdot cm^{-1}$. A plot of the increase in absorbance at 570 nm (17 540 cm^{-1}) as a function of the Hammett acidity function ($-H_o$) yields a pK_a of −5.75, within experimental error of previous determinations.[9]

II. NMR Spectroscopy. Although absorption spectra exhibit only slight changes in the 1−3 pH range, NMR spectra clearly reveal proton dependent changes. To achieve the necessary concentration, ca. 10^{-2} M, all NMR experiments made use of the nitrate salt, $[Ru(bpy)_2(dpp)](NO_3)_2$, dissolved in D_2O to

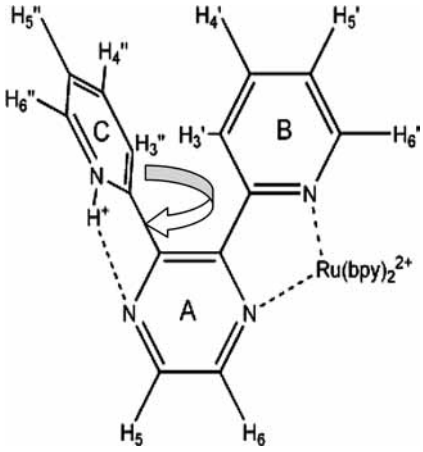

Figure 2. Structure of the protonated complex, $Ru(bpy)_2(dpp)H^{3+}$, showing rotation of pendant pyridyl ring and resulting steric repulsion between hydrogens C3" and B3′.

which increasing amounts D_2SO_4 were added. Consistent with the aromaticity of the ligands, the chemical shifts of all protons in $Ru(bpy)_2(dpp)^{2+}$ fall within the 6 to 9 ppm aromatic region. Coordination to the metal and the subsequent countervailing effect of metal-to-ligand back-bonding shift the proton resonances to lower ppm relative to those of the free ligands. Assuming the area of the lowest-field doublet at 8.75 ppm corresponds to a single proton, the ^1H NMR spectrum of $Ru(bpy)_2(dpp)^{2+}$ in D_2O integrates to the expected 26 protons. $^1H-^1H$ COSY reveals the protons are distributed among seven independent ring-spin systems: four in the bpy ligands and three in the dpp ligand. Although the shifts differ slightly, the proton assignments agree with those reported for $[Ru(bpy)_2(dpp)](PF_6)_2$ in acetonitrile.[13]

Five of the 26 protons shift to lower field as the acidity of the solution increases (Supporting Information). Four protons, C3"−C6" (Figure 2), correspond to the protons on the dpp pendant pyridyl ring and one, starting at 7.2 ppm corresponds to B3′ on the coordinated pyridyl ring of dpp. Plots of pD versus percent change in chemical shift for these resonances are all sigmoidal, with a common inflection point at a pD of 1.52 ± 0.03.

Assuming the data represents one protonation equilibrium (vide infra), extracting the equilibrium constant for protonation from NMR shifts rests on the maximum value of the shift, $\Delta\delta_{max}$. Unfortunately, at the higher acid concentrations needed, it was difficult to precisely determine $\Delta\delta_{max}$ because of loss of spectral resolution. Consequently, a nonlinear, least-squares fitting was used to extract $\Delta\delta_{max}$ and K_a, where K_a refers to the acid dissociation constant for the complex,

$$Ru(bpy)_2(dppH_{py})^{3+} \rightleftarrows Ru(bpy)_2(dpp)^{2+} + H^+ \quad (1)$$

$Ru(bpy)_2(dppH_{py})^{3+}$ designates protonation of the nitrogen on the peripheral dpp pyridyl ring. For a monoprotonated complex dissociating, the shift in the proton resonance, $\delta_{observed}$, as a function of $[H^+]$ ($[D^+]$) is given by

$$\Delta\delta_{observed} = [(\delta_{bound} - \delta_{free})]\frac{1}{2[H^+]_o}[([H^+]_o + [Ru]_o + K_a) - \sqrt{([H^+]_o + [Ru]_o + K_a)^2 - 4[Ru]_o[H^+]_o}] \quad (2)$$

where δ_{bound} and δ_{free} designate the shifts of the observed protons with and without acid and as a function of $[H^+]$, respectively. $[Ru]_o$ represents the initial complex concentration, generally 10^{-2} M, and $[H^+]_o$ (actually $[D^+]_o$) represents a given hydrogen ion concentration. Constraining K_a to be positive and $\Delta\delta_{max} \geq \Delta\delta_{free}$, eq 2 provides an excellent fit of the observed shifts (Figure 3) for each of the shifting protons. Each proton shifts to a different extent with increasing acidity, yet the average pK_a value extracted from each of the fits (Figure 3), 1.52 ± 0.03, agrees and matches the common inflection point, 1.52 ± 0.03, providing additional confidence in the fitting procedure. The calculated pK_a must be adjusted for the isotope effect given that the experiments were done in deuterated solution, giving an approximate pK_a of 1.12.[14]

III. Steady-State and Time-Resolved Emission Spectroscopy. Excitation of aqueous solutions of $Ru(bpy)_2(dpp)^{2+}$ with light of ≤540 nm leads to an emission with a maximum at 705 nm (14 200 cm^{-1}). In basic solution, pH ≥8, the emission intensity at 705 nm, emission lifetime and quantum yield are independent of pH. However, as the pH declines each of these factors declines with the most prominent changes beginning around pH 5. Plots of the relative lifetimes (τ/τ_o) and quantum efficiencies (Φ/Φ_o) versus pH have common inflection points at pH 4.5 (Supporting Information).

At pH 1, the emission at 705 nm is gone and the spectrum consists of two weak emissions with maxima at 620 nm (16 100 cm^{-1}) and 735 nm (13 600 cm^{-1}). The relative intensities of the emissions depend on the excitation wavelength with the 620 nm emission increasing as the excitation wavelength shifts from the dpp localized MLCT transition to the bpy localized MLCT transition. The emission maxima are independent of whether the solution is acidified with HNO_3 or H_2SO_4, and both persist in acidified solution with no measurable change in intensity until the solution is made 1 M in acid. Beyond this point, the 735 and 620 nm emissions exhibit different dependencies upon $[H^+]$. The 735 nm emission declines with further increases in $[H^+]$, whereas the 620 nm emission intensity is initially independent of further increases in $[H^+]$ but eventually declines and disappears at higher $[H^+]$. The 620 nm emission, which is described in a recent report,[15] is assigned to a competitive bpy-localized MLCT emission and is not discussed in any further detail here. This discussion focuses on the 735 nm emission, which becomes evident as the 705 nm emission intensity declines and is detectable within a window of $[H^+]$ ranging from ca. 10^{-4} M to ca. 2 M (Figure 4).

In 12.5 M H_2SO_4, regardless of the excitation wavelength, no emissions are detectable from room temperature, deareated solutions of $Ru(bpy)_2(dpp)^{2+}$. At this high acidity, the solution is purple and the initially present 428 and 476 nm MLCT absorptions are replaced by the 573 nm absorption with a shoulder at ca. 380 nm. Although high acidities are needed to completely quench the emissivity of the complex and produce these changes in the complex's absorption spectrum, it is important to emphasize that these changes are reversible on the addition of a base.

The lifetime and intensity quenching of the 705 nm emission from $(bpy)_2Ru(dpp)^{2+}$ exhibit a complex dependence on $[H^+]$ (Figure 5). The Stern−Volmer plot is initially quite steep followed by significant negative deviations. For $[H^+] \leq 10^{-4}$M, intensity and lifetime quenching are within experimental error. Over the pH range from 5 to 3 a linear plot yields $K_{sv} = 583 \pm 60$ M^{-1}, which is within experimental error of that previously determined over the same pH range.[8] Taking 116 ± 12 ns as the lifetime of $*(bpy)_2Ru(dpp)^{2+}$ in pH 7 buffer solution, the

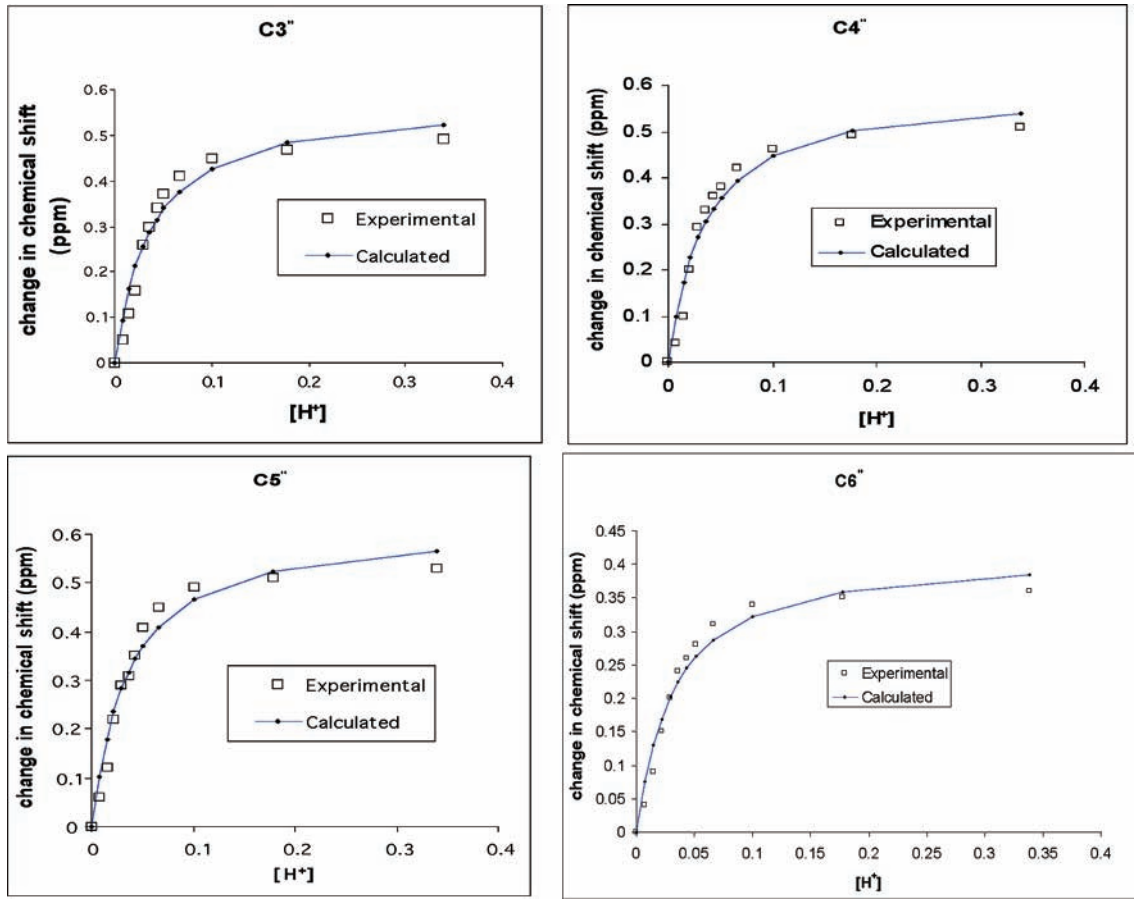

Figure 3. Change in the chemical shifts as a function of $[D^+]$ (□) and change expected based on eq 2 (—).

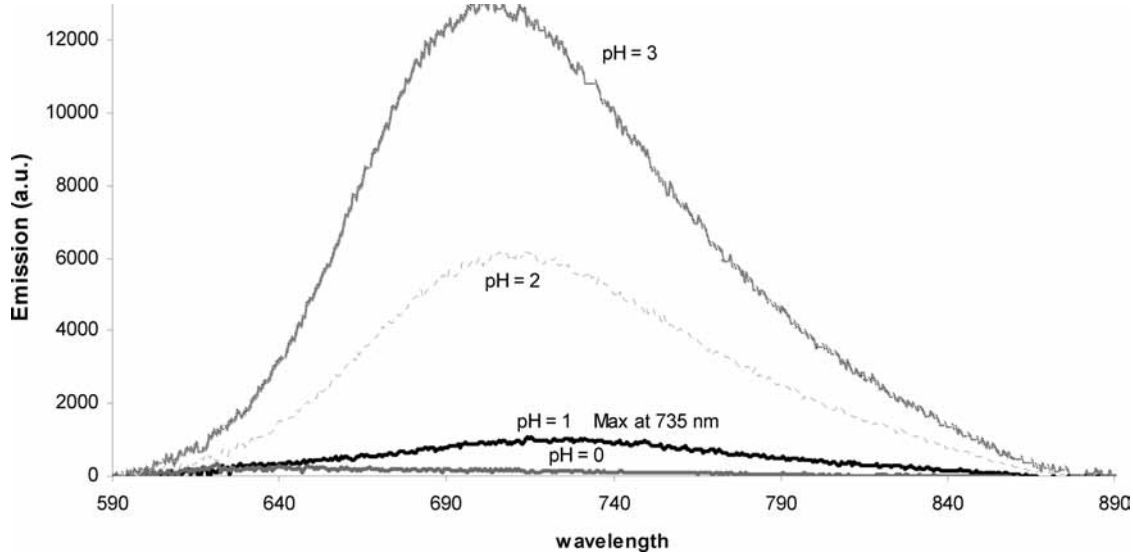

Figure 4. Emission spectra of $Ru(bpy)_2(dpp)^{2+}$ at low pH. The red shift becomes discernible at pH 2, and the maximum shifts to 735 nm at pH 1.

relationship $K_{SV} = k_b\tau$ yields $5.1 \pm 0.5 \times 10^9$ $M^{-1}\cdot s^{-1}$ as the bimolecular rate constant for protonation of the excited complex. Attempts to fit the entire range of $[H^+]$ examined with the more general form of the Stern−Volmer expression:[16]

$$\frac{I_o}{I} = \frac{1 - k_b\tau_{unprotonated}[Q]}{1 - \gamma k_b\tau_{protonated}[Q]} \quad (4)$$

where

$$\gamma = \frac{I'_1\tau_{unprotonated}}{I_1\tau_{protonated}} \quad (5)$$

failed. In this model, which might account for the overlapping 705 and 735 nm emissions, I'_1 is the emission intensity from

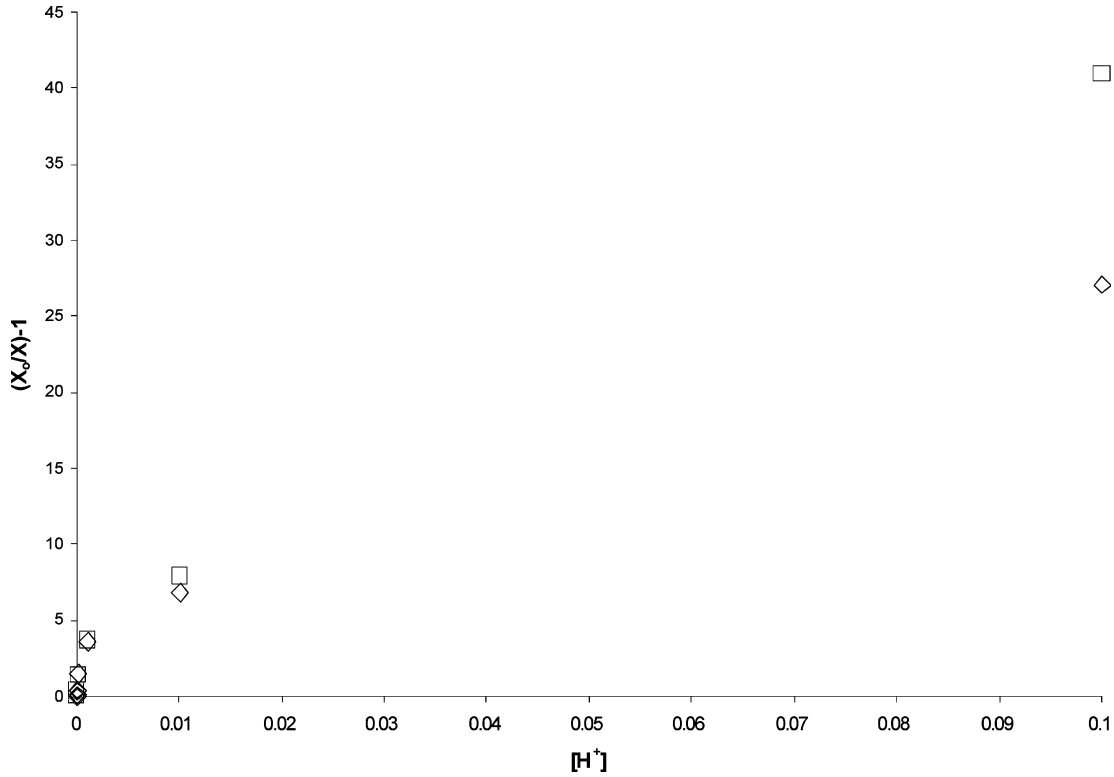

Figure 5. Stern−Volmer plots of the 705 nm emission quantum yields (□) and lifetimes (◇) vs [H^+]. Emission quantum yields were measured with 488 nm excitation and the lifetimes with 532 nm excitation.

the protonated form at 705 nm, I_l is the intensity from the unprotonated complex at 705 nm, k_b is the bimolecular rate constant for protonation, and $\tau_{unprotonated}$ and $\tau_{protonated}$ are the respective lifetimes. Nonlinear regression produced reasonable fits at the extremes of the data but failed to reproduce the entire range examined.

IV. 735 nm Emission. At pH values ≤4, the emission spectrum is a composite of two, overlapping emissions and any attempt to analyze the intensity quenching is biased by the presence of the second, red-shifted emission.[17] The 735 nm emission arises from the monoprotonated complex (vide infra) and its contribution, as well as that of $Ru(bpy)_2(dpp)^{2+}$, was calculated from the individual spectra of the two species. The emission spectrum of the unprotonated complex, designated ξ_{unp}, was taken to be that recorded at pH 8 where only the unprotonated complex is present and no further change in the spectrum is evident at higher pH's. The emission spectrum of the monoprotonated complex, designated ξ_p, was approximated by the spectrum at pH 1 because no further red shifts occur at lower pH. Because NMR spectra suggest that both the unprotonated and monoprotonated complexes are present between pH 8 and 1, with each able to undergo excited-state protonations, by combining these spectra in varying ratios and fitting the resulting composite spectra to the observed spectra according to:

$$I_{observed} = f_p\xi_p + (1 - f_p)\xi_{unp} \quad (6)$$

the contributions from the monoprotonated and unprotonated complexes in the excited state can be determined and compared to the fractions available in the ground state as defined by the pK_a. Sigmoidal fits of plots of these fractions at each pH have inflection points where they cross at pH ~3.1 (Supporting Information). This value is interpretable as a *pK_a of 3.1, but confidence in the fits is limited by the few points available.

With the products $f_p\xi_p$ and $(1 - f_p)\xi_{unp}$, the contributions of each species can be tracked. At pH > 5, the 705 nm emission from $(bpy)_2Ru(dpp)^{2+}$ is the principal contributor to the composite spectrum, whereas the 735 nm emission from the monoprotonated complex appears between pH 4 and 3, increases in intensity, and then declines as the pH decreases to 0 (Figure 6).

Taking the 735 nm intensity at pH 2 as the maximum intensity, a plot of I_o/I versus [H^+], based on the extracted emission spectra at pH 2, 1, and 0, is linear yielding a Stern−Volmer constant of 13.7 ± 1.4 M^{-1} for the quenching of the 735 nm emission from the monoprotonated complex, $(bpy)_2Ru(dppH)^{3+}$, by H^+ (insert in Figure 6).

Exciting room temperature, pH 1 (0.1 M HNO_3), N_2 saturated, aqueous solutions of $Ru(bpy)(dpp)^{2+}$ with a 400 nm, 16 ps (fwhm) pulse, and monitoring the 450−750 nm region confirms that the 735 nm emission decays within the duration of the excitation pulse. Thus, the lifetime of the 735 nm emission, ≤16 ps, precluded measuring the dependence of lifetime on [H^+]. Taking 16 ps as an upper bound on the excited-state lifetime of this monoprotonated complex, and $K_{SV} = 13.7 \pm 1.4\ M^{-1}$, the relationship $K_{SV} = k_b\tau$ yields $8.6 \times 10^{11}\ M^{-1}s^{-1}$ as the bimolecular rate constant for protonation of the monoprotonated, excited complex.

V. Quantum Yields. The quantum efficiency of the 705 nm emission from the unprotonated complex $Ru(bpy)_2(dpp)^{2+}$ was measured relative to $Ru(bpy)_3^{2+}$ in water. On the basis of a pK_a of 1.12, at pH 5, ≥99.99% of the complex is present as $Ru(bpy)_2(dpp)^{2+}$, and the emission spectrum consists of only the 705 nm emission from the unprotonated complex. Taking the quantum efficiency of emission from room temperature, 22 ± 1 °C, N_2 saturated, aqueous solutions of $Ru(bpy)_3^{2+}$ in water

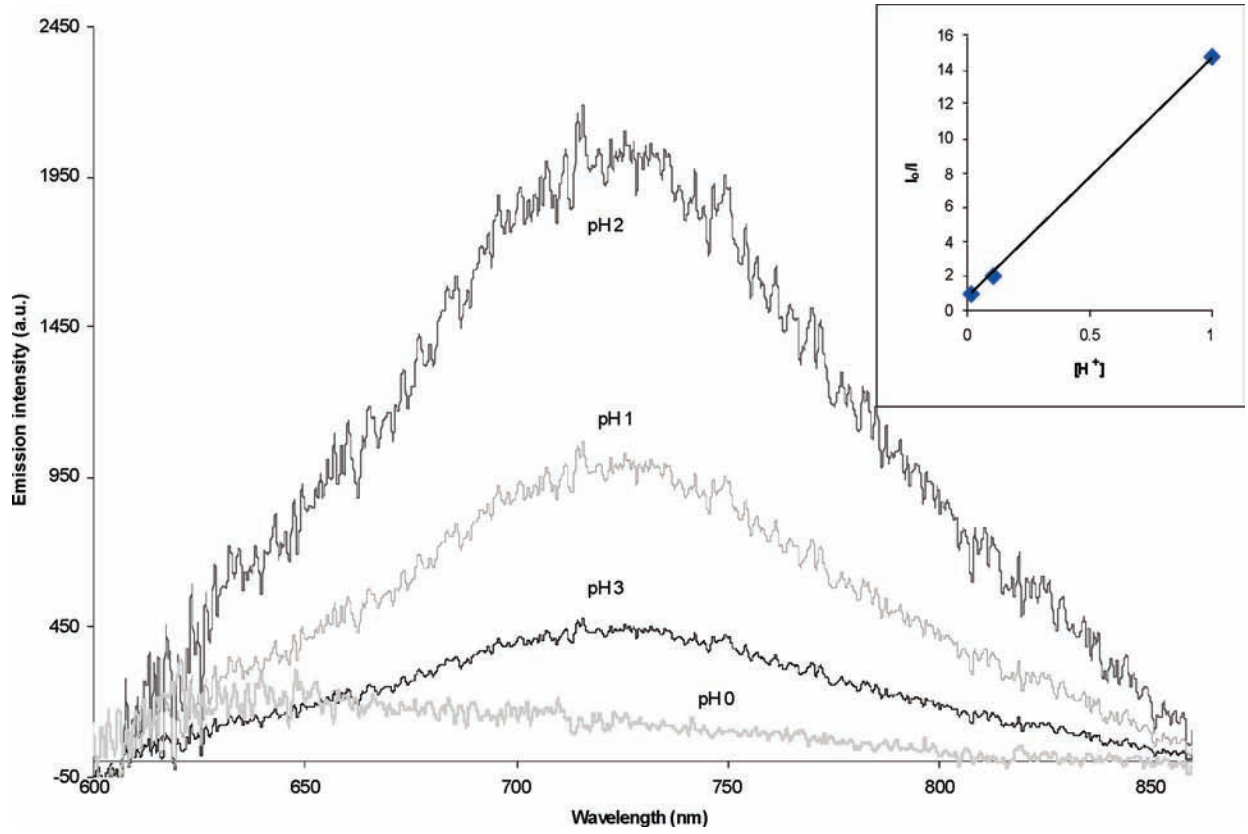

Figure 6. Extracted 735 nm emission at various pH values. The 735 nm emission begins to contribute to the overall emission spectra at pH 3, increases in intensity as the pH reduces to 2, then declines.

TABLE 1: Photophysical Parameters and Radiative and Nonradiative Rates Constants for $Ru(bpy)_2(dpp)^{2+}$ and $Ru(bpy)_2(dppH)^{3+}$

	λ_{em}(nm)	Φ_{em}	τ (seconds)	$k_r s^{-1}$	$k_{nr} s^{-1}$
$Ru(bpy)_2(dpp)^{2+}$	705	$1.98 \pm 0.20 \times 10^{-3}$	$1.26 \pm 0.07 \times 10^{-7}$	$2.0 \pm 0.3 \times 10^{4}$	$9.8 \pm 1 \times 10^{6}$
$Ru(bpy)_2(dppH)^{3+}$	735	$4 \pm 1 \times 10^{-9}$	$\leq 1.6 \pm 0.2 \times 10^{-11}$ ($\leq$16 ps)	$\geq 2.5 \pm 0.3 \times 10^{2}$	$\geq 6.2 \pm 1 \times 10^{10}$

to be 0.0429 (averaged from several references[18]), the gradient method using a series of concentrations $\leq$0.10M[11] yields $1.98 \pm 0.20 \times 10^{-3}$ as the quantum efficiency of the 705 nm emission from the unprotonated complex $Ru(bpy)_2(dpp)^{2+}$, designated $\Phi_{em}{}^{u}$. The 735 nm emission from the protonated complex was then measured from a deaerated, aqueous solution containing the same concentration of $Ru(bpy)_2(dpp)^{2+}$ but 1.0 M in HNO_3. With 1 M HNO_3, $\geq$93% of the complex is present as the protonated complex, $Ru(bpy)_2(dppH)^{3+}$, and the emission spectrum consists of the 620 and 735 nm emissions from the protonated complex. The difficulty is the huge difference in the intensity from the protonated complex relative to that from the unprotonated complex or a $Os(bpy)_3{}^{2+}$ standard. To compensate for the intensity difference, the 735 nm emission from the protonated complex $Ru(bpy)_2(dppH)^{3+}$ was measured relative to the 705 nm emission from $Ru(bpy)_2(dpp)^{2+}$ utilizing the camera gain to compensate for the intensity difference.[19] Taking $\Phi_{em}{}^{u}$ for the unprotonated complex to be $1.98 \pm 0.20 \times 10^{-3}$, the quantum efficiency of the 735 nm emission from the protonated complex, designated $\Phi_{em}{}^{p}$, was calculated to be $4 \pm 1 \times 10^{-9}$. As noted, no emission attributable to the diprotonated complex, $Ru(bpy)_2(dppH_2)^{4+}$, could be detected from highly acidic $\geq$5 M H_2SO_4 solutions of the complex. Table 1 summarizes the emission data for the unprotonated and monoprotonated complexes and the respective values of the radiative, k_r, and nonradiative, k_{nr}, rate constants derived from the relationships $\tau = 1/(k_r + k_{nr})$ and $\Phi_{em} = k_r/(k_r + k_{nr})$.

Discussion

Our model describing the individual molecular steps indicated by the spectroscopic and quenching data accumulated in these experiments are summarized in Scheme 1.

I. Ground-State Equilibria: Monoprotonation. NMR spectra clearly show proton dependent changes at pH values intermediate between those observed in the absorption and emission spectra of $Ru(bpy)_2(dpp)^{2+}$. The downfield shifts of the pyridyl C3", C4", C5", C6" protons with increasing acidity (Figure 2) are consistent with the deshielding presence of a positive charge at the dpp peripheral pyridyl nitrogen. The shifts of the protons attached to 3′ and 3" on rings B and C respectively specifically point to protonation at this imine nitrogen. Whereas the downfield shift of the C3" proton is consistent with deshielding due to the presence of a positive charge on the peripheral pyridyl nitrogen, the downfield shift of B3′ is unexpected because this proton is on the coordinated pyridine that no longer possesses a free acid−base site. Coordination of dpp to Ru(II) forces the pyrazinyl and coordinated pyridyl rings (rings A and B in Figure 2) to be planar or close to planar, whereas the pendant pyridyl ring (C) is expected to remain out of the plane of the other rings. Indeed, the crystal structure of $[(bpy)_2Ru(dpp)]Cl_2$ confirms the pendant pyridyl ring is out of the plane of the coordinated pyrazinyl and pyridyl rings with a dihedral angle of 106.8°.[13] Closely perpendicular to the coordinated pyridyl ring (B), the ring current

SCHEME 1: Proposed Model for the Ground- and Excited-State Processes Involving Protonation of $Ru(bpy)_2(dpp)^{2+}$ and $Ru(bpy)_2(dppH)^{3+}$ [a]

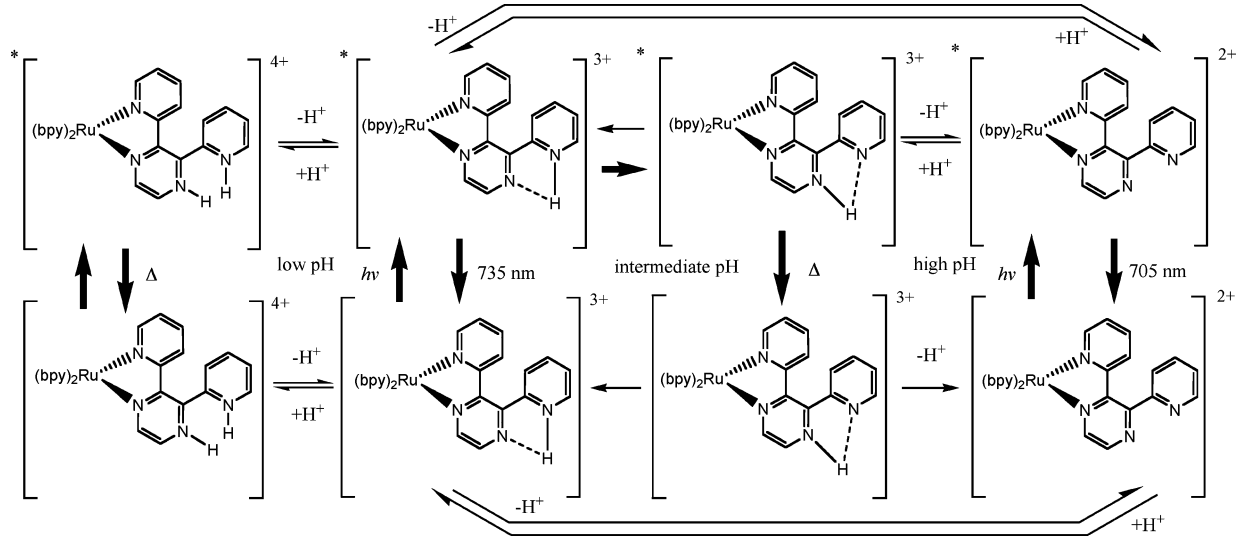

[a] Dissociation steps are shown from left to right with the top row describing excited-state equilibria and the bottom row ground-state equilibria. The scheme begins with the unprotonated species at the lower right-hand corner.

of the pendent pyridyl (C) shields the B3′ proton. The downfield shift of the B3′ proton concomitant with increasing acidity implies either a decline in the ring current effect, which would occur if the pendant pyridyl twists on protonation (circular arrow in Figure 2) to increase intramolecular hydrogen bonding with the peripheral pyrazinyl nitrogen or that the pendant pyridyl ring puckers.[20] Either situation lessens the shielding of the ring current of the pendant pyridyl (C) on the B3′ proton. Twisting is thought to be the dominant effect; however, because twisting not only reduces the ring current effect on B3′, but also produces a steric, deshielding interaction between the B3′ hydrogen and the C3" hydrogen as the pendant ring approaches planarity. In fact, the largest shifts with increasing acidity are those of C3" and B3′ (Supporting Information), which are consistent with protonation of the pendent pyridyl ring and its twisting to achieve a more planar, cyclic structure with the newly attached proton hydrogen bonded to the pyrazinyl nitrogen. This is not to say the proton is equally shared between the two sites: collectively, the evidence discussed below suggests, at least in the ground state, it is principally associated with the pendant pyridyl nitrogen. It is important to recognize that the pendant pyridyl ring completely twists upon protonation — the gradual change in the NMR does not reflect increasing twisting with increasing $[H^+]$ but the time-average of the proportion of protonated to nonprotonated species with increasing $[H^+]$.

Consequently, the first protonation of ground-state $Ru(bpy)_2(dpp)^{2+}$ occurs at the peripheral dpp pyridine nitrogen, and the protonated complex, designated $Ru(bpy)_2(dppH_{py})^{3+}$, exhibits a pK_a of 1.12 ± 0.03 when adjusted for the isotope effect. The value is significantly smaller than that for pyridinium ion, $pyH^+ \rightleftarrows py + H^+$, $pK_a = 5.23$, suggesting that either the cationic metal center inductively reduces electron density at the peripheral dpp pyridine nitrogen and/or facilitates proton dissociation through cationic repulsion of the proton by the positive Ru^{2+} center. The latter is thought to be the dominant, though not exclusive, factor because protonation occurs with little change in the complex's MLCT absorptions. The large dihedral angle is expected to reduce any electronic coupling between the metal center and the pendant pyridyl ring. Thus, $Ru(bpy)_2(dpp)^{2+}$ is unique because of the minimal spectral change accompanying protonation of the dpp peripheral pyridine; for the energies of the MLCT absorptions, that to the bpy shifts 200 cm^{-1} to higher energy, and that to dpp shifts by $\leq$600 cm^{-1} to lower energy with the intensities (or allowedness) of the absorptions increasing by a mere 17% to bpy, and decreasing by 10% to dpp. In fact, the changes are so small they were originally assigned to ionic strength effects rather than protonation.[9] Minimal electronic coupling seems inconsistent with extensive charge reorganization due to the inductive effect of the Ru^{2+}, especially because the pendant pyridyl ring is twisted with regards to the rest of the dpp ligand. Furthermore, although NMR suggests that $Ru(bpy)_2(dppH_{py})^{3+}$ adopts a cyclic structure with the proton intramolecularly shared between the peripheral dpp pyrazinyl and pyridyl nitrogens, these nominal changes in the absorption spectra suggest the proton is not equally shared but remains principally associated with the pyridyl nitrogen. Nonetheless, it has a profound effect on the emissivity and decay of the excited complex (vide infra).

II. Ground-State Equilibria: Diprotonation. Reversible on addition of a base, the dramatic change from reddish-orange to violet occurring at high acidity, $H_0 < -4$ and corresponding appearance of the 573 nm absorption were originally assigned to the first protonation of the complex.[8,9] Occurring with increasing acidity after the protonation evident in the NMR (Figure 7), however, clearly shows the 573 nm absorption corresponds to the second protonation of the complex and formation of $Ru(bpy)_2(dppH_2)^{4+}$.

$$Ru(bpy)_2(dppH_{py})^{3+} + H^+ \rightleftarrows Ru(bpy)_2(dppH_2)^{4+} \quad (7)$$

The second protonation occurs at the pyrazinyl nitrogen and, as a component of that portion of dpp coordinated to Ru(II) produces a larger change in the MLCT transition energy, $\Delta E = 2900$ cm^{-1}, relative to that which occurs on protonation of peripheral dpp pyridine, $\Delta E = 600$ cm^{-1}. These results complement resonance Raman spectroscopy[21] and collectively indicate that the charge transferred in the MLCT to dpp is principally localized at the dpp pyrazinyl group. The minimal involvement of the pendant pyridine is attributed to its orthogonality to the coordinated portion of dpp.

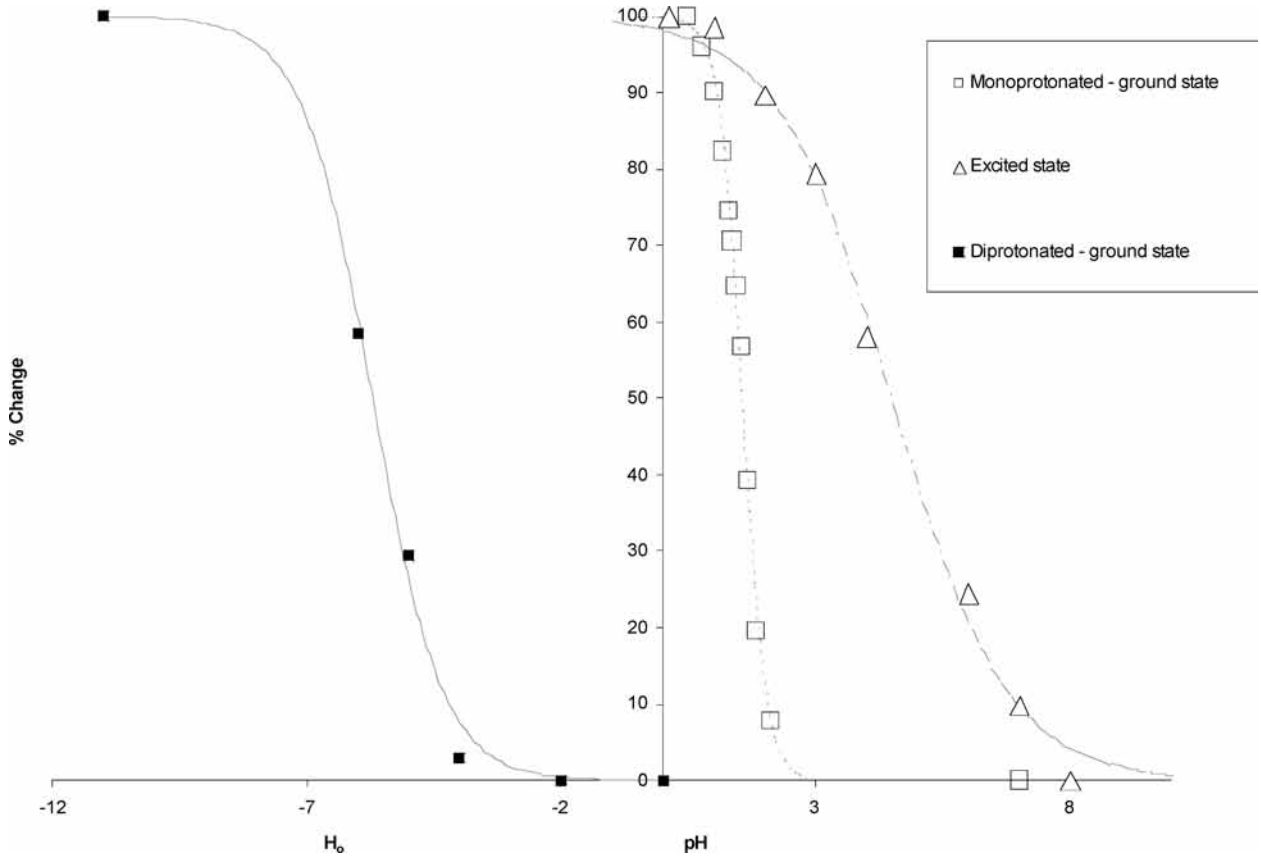

Figure 7. Ground- and excited-state titration curves for $Ru(bpy)_2(dpp)^{2+}$. From left to right, the curves correspond to diprotonation (-■-) of $Ru(bpy)_2(dpp)^{2+}$, monoprotonation of $Ru(bpy)_2(dpp)^{2+}$ (--□--), and protonation of the excited complex (-•Δ-•) derived from UV−vis, NMR, and emission quenching, respectively.

III. Emission Spectra. The ground-state acid−base equilibria of $Ru(bpy)_2(dpp)^{2+}$ (Figure 7) establish the presence of $Ru(bpy)_2(dpp)^{2+}$, $Ru(bpy)_2(dppH_{py})^{3+}$, and $Ru(bpy)_2(dppH_2)^{4+}$ in aqueous solution as a function of $[H^+]$. The occurrence of the 705 nm emission at high pH, and in aprotic solvents confirms its assignment to an emission from the unprotonated complex.[8,9] As $[H^+]$ increases, the 705 nm emission intensity declines and is replaced by a weaker emission centered at 735 nm. The 735 nm emission appears within a window of hydrogen ion concentrations, $0.001\ M \leq [H^+] \leq 1M$, close to the pH window over which the equilibrium evident in the NMR occurs (Figure 7) suggesting that the 735 nm emission arises from $Ru(bpy)_2(dppH_{py})^{3+}$ with the proton attached to the dpp peripheral nitrogen.

The initial difficulty with this interpretation is that, based on the acid dissociation constant for $Ru(bpy)_2(dppH_{py})^{3+}$ obtained by NMR, at pH = 2, where the 735 nm emission intensity reaches a maximum (Figure 6), only 12% of the $Ru(bpy)_2(dpp)^{2+}$ exists as $Ru(bpy)_2(dppH_{py})^{3+}$, but it accounts for nearly 95% of the emission. Three factors can account for this. First, $Ru(bpy)_2(dppH_{py})^{3+}$ itself will absorb the excitation light with nearly the same efficiency, thus reducing the amount of emission expected from $Ru(bpy)_2(dpp)^{2+}$ by an additional 12%. Second, $Ru(bpy)_2(dpp)^{2+}$ will continue to be quenched by $[H^+]$ at the pyrazinyl nitrogen. With a K_{SV} of 583 M^{-1}, this translates into a reduction of the emission by an additional 87%, leading to total reduction of about 93%. Yet, at pH 2, the extracted 705 emission is reduced by 99.7% to 0.3% of I_o. Therefore, the third factor is that excitation of the unprotonated complex may also lead to formation of the monoprotonated complex *at the pyridyl nitrogen* in the excited state. This is possible because Su and Kincaid have shown using resonance Raman that electron redistribution upon population of the MLCT is primarily to the pyrazine portion of the dpp, but is asymmetric with a finite, small portion onto the pendant pyridyl ring.[21] This portion may be sufficient to translate into an enhanced basicity in the excited state.

The change in basicity upon excitation, ΔpK_a, can be estimated from the Förster cycle:[22]

$$pK_a^* - pK_a = \Delta pK_a = 2.09 \times 10^{-3}(\upsilon_B - \upsilon_{BH+})/cm^{-1} \quad (8)$$

$\upsilon_B - \upsilon_{BH+}$ represents the difference in energy between the two forms, and, consequently, the estimation is very sensitive to the wavelengths chosen. Implicit in the Förster cycle is the assumption that only one protonation site is being considered. Making use of the different emission maxima at 705 and 735 nm results in an estimated ΔpK_a of 1.21, which translates into an estimated $*pK_a$ of 2.33. Interestingly, on the basis of the rough difference between the expected emission intensity at 705 nm at 7% of I_o and the actual, which is 0.3% of I_o, it is possible to calculate the $*pK_a$ needed to translate the difference, 6.7%, to the monoprotonated species in the excited state at pH 2, which would be 3.32. This is not far from the inflection point in of 3.1 (See Supporting Information), which could be interpreted as the $*pK_a$ of the pyridyl nitrogen. This gives further credence to the suggestion that an excited-state monoprotonation reaction can occur at either of the peripheral nitrogens, with the pyrazinyl dominating at high pH, and a competition ensuing with increasing $[H^+]$ as the pH is lowered.

To summarize, the 735 nm emission is assigned to that from $Ru(bpy)_2(dppH_{py})^{3+}$ for the following reasons: (1) The 735 nm emission appears and disappears within a pH range corresponding to the first protonation (Figure 7); (2) the small change in emission energy, $\Delta E = 579\ cm^{-1}$ is essentially equivalent to the change in energy corresponding to the shifts in the dpp localized MLCT absorptions, $\Delta E = 600\ cm^{-1}$, that accompany the first protonation; and last, (3) the dramatic increase in the nonradiative rate constant (Table 1) implies that protonation of the peripheral pyridine increases vibronic coupling to the surrounding solvent thereby enhancing the dissipation of the excitation energy to the solvent medium and reducing the overall emissivity compared to the unprotonated complex.

The minimal changes in the absorption spectra that accompany the first protonation are in sharp contrast to the spectral changes accompanying the second protonation. Protonation of $Ru(bpy)_2(dppH_{py})^{3+}$ adds the second proton to peripheral dpp pyrazinyl nitrogen. The solution changes from orange-red to violet and the 422 and 490 nm MLCT absorptions are replaced by a band at 573 nm with a shoulder at 380 nm. The 573 nm absorption is assigned to the dpp localized MLCT and, reflecting the increased positive charge due to diprotonation, is shifted to lower energy. The shoulder at 380 is assigned to the bpy localized MLCT absorption, which occurs at higher energy as a result of the inductive effect of diprotonated dpp ligand. In spite of the strong acidity needed to induce the second protonation, the spectral changes are quantitatively reversible on addition of NaOH. Quantitative reversibility places the molar extinction coefficient of the 573 nm absorption at $1.82 \pm 0.01 \times 10^3\ M^{-1}\cdot cm^{-1}$. The absence of any detectable emission in the 700−900 nm range from these strongly acidic, violet solutions implies the quantum yield of emission from $Ru(bpy)_2(dppH_2)^{4+}$, is $\leq 4 \times 10^{-9}$, or the complex is nonemissive. The critical point is that the second protonation is at the pyrazinyl nitrogen, which, being directly coupled to the MLCT system, expectedly leads to these dramatic shifts in the absorbance and quenches all emissivity, in stark contrast to protonation at the pendant pyridyl ring.

IV. Quenching of $Ru(bpy)_2(dpp)^{2+}$. The deviation in the lifetime and intensity quenching of $Ru(bpy)_2(dpp)^{2+}$ by H^+ (Figure 5) clearly indicates both static and dynamic processes. The general version of the Stern−Volmer eq 4 fits both static and dynamic quenching, *but only for corresponding chemical reactions, in this case protonations, that occur at the same site.* Consequently, any attempt to resolve the proton quenching dynamics of a complex possessing two acid−base sites in close proximity rests on identifying the site at which the quenching reaction occurs.

At pH values down to 5, $Ru(bpy)_2(dpp)^{2+}$ is present >99.9%. Excitation leads to radiative deactivation at 705 nm and with increasing acidity the possibility of proton quenching at either the pyrazinyl or pyridyl nitrogens. In this high pH cycle (Scheme 1), we assign any excited-state protonation to formation of the protonated complex at the pyrazinyl nitrogen, $*Ru(bpy)_2(dppH_{pz})^{3+}$, based on the following evidence and reasoning: 1) the absence of any indication of the 735 nm emission from $Ru(bpy)_2(dppH_{py})^{3+}$; 2) the majority of electron density due to population of the MLCT resides on the pyrazinyl nitrogen which would translate into the strongest enhancement of basicity (vide infra); 3) protonation at the pyrazinyl nitrogen which is coupled strongly to the MLCT explains the deactivation and quenching of any emission; and, 4) lifetime and intensity quenching match consistent with a diffusion process. Using the Stern−Volmer constant, $K_{SV} = 583 \pm 60\ M^{-1}$, and the $*Ru(bpy)_2(dpp)^{2+}$ emission lifetime at pH 7, 116 ± 12 ns, yields $5.1 \pm 0.5 \times 10^9\ M^{-1}s^{-1}$ as the bimolecular rate constant for protonation of the excited complex at the pyrazinyl nitrogen. The rate constant is smaller than rate constants reported for proton transfer to uncharged molecules, suggesting that electrostatic repulsion between the +2 cationic complex and the proton curtails the quenching process. Deactivation of $*Ru(bpy)_2(dppH_{pz})^{3+}$ will lead to immediate deprotonation at pH levels above 5.

As the pH is lowered further, unprotonated complex is converted to the monoprotonated complex in the ground state, which accounts for deviations between lifetime (diffusional) and intensity (total) quenching. In essence, the chromophore that accounts for the 705 nm emission is removed by protonation and this is usually referred to as "associational quenching." The remaining unprotonated complex is further quenched by the increasing presence of $[H^+]$. Additionally, at pH 4 and below, the enhanced basicity at the *pyridyl* nitrogen becomes competitive, accounting for formation of $*(bpy)_2Ru(dppH_{py})^{3+}$ in the excited state and thus appearance of the 735 nm emission in greater fractions. These factors continue to account for the stark disappearance of any emission from the unprotonated complex despite its pre-excitation presence down to pH 1.

V. Excited-State Enhanced Basicity. There is an additional consideration that bolsters the contention that the MLCT inverts the relative basicities of the peripheral nitrogens. In other words, the increase in basicity at the pyrazinyl nitrogen, being both strongly coupled to the MLCT and the primary venue for increased electron density upon population of the MLCT, is so large as to make it significantly more basic than the pyridyl in the excited state and thus the location for proton quenching at high pH. The apparent pK_a* from the emission titration in Figure 7 is 4.5; however, there is uncertainty as to which protonation site it refers to and whether the value is accurate. Uncertainties may arise when either of the unprotonated or protonated forms is non- or weakly emissive, when the lifetimes are so short that an excited-state equilibrium is not attained and possibly when the lifetimes are different. As mentioned, the Förster cycle can be used to estimate the ΔpK_a and thus $*pK_a$ when there are uncertainties associated with obtaining $*pK_a$ values from the inflection points of emission titration curves. However, again, implicit in the Förster cycle is the assumption that only one protonation site is being considered and that the change in basicity is for corresponding protonation steps in the ground and excited states. For protonation of the pyrazinyl nitrogen, this is not possible because it is the second protonation in the ground state but, according to our model, the first protonation takes place in the excited state. A rough estimate might be obtained using 476 and 573 nm as the two absorption maxima for the unprotonated and diprotonated forms respectively. With a K_a of $H_o = -5.75$ for protonation of the pyrazinyl nitrogen, ΔpK_a is calculated to be 7.43, and thus pK_a* is estimated at 1.68. This is almost certainly a lower limit − although monoprotonation has minimal effect on the electronic spectrum, it does affect the ease with which the pyrazinyl nitrogen is subsequently protonated in the ground state. Formation of the diprotonated species is unfavored by electrostatic repulsion to form a +4 species, so if one were considering the basicity of the pyrazinyl nitrogen alone, absent the pendant pyridyl ring, it would be expected to be higher than −5.75.[23] This would translate to a higher estimated pK_a*. On the other hand, a good estimate can be obtained from the first pK_a of the pyrazinyl nitrogen of the well-characterized analogue, $[(bpy)_2Ru(bpz)]^{2+}$ (where bpz = 2,2′-bipyrazine), which was determined to be

−1.6.[24] Using the calculated ΔpK_a value of 7.43 translates this into a $*pK_a$ of 5.83.

In our estimation, ΔpK_a and pK_a* are only useful to the extent that they indicate how an energetic change can translate into a particular chemical reaction. Because the diffusion-controlled forward rate for protonation is likely to be fairly similar in both the ground and excited states, what translates into excited-state enhanced basicity, or an increase in pK_a* with respect to pK_a, is more related to a decrease in the rate constant for *deprotonation* in the excited state relative to the ground state. In simplistic terms, features of the excited state, such as increase in electron density at a basic site, allow for the species to hold on better to the proton or some other species like a metal cation.

VI. Quenching of the Monoprotonated Complex, $Ru(bpy)_2(dppH_{py})^{3+}$. At pH values below 4, the 735 nm emission appears, increases to at maximum at pH 2, and then declines. As mentioned, the appearance of the 735 nm emission is accounted for by the equilibrium formation of the monoprotonated species in the ground state prior to excitation, and the additional formation in the excited state due to enhanced basicity of the pyridyl nitrogen. From pH 2 to 0, quenching of the 735 nm emission (Figure 6) exhibits a linear dependence on $[H^+]$ and yields a Stern−Volmer constant of 13.7 ± 1.4 M^{-1}. Although the short lifetime of $*Ru(bpy)_2(dppH_{py})^{3+}$, <16 ps, precluded measuring lifetime quenching, the relationship $K_{SV} = k_b\tau$ yields 8.6×10^{11} $M^{-1}s^{-1}$ as the bimolecular rate constant for protonation of $*Ru(bpy)_2(dppH_{py})^{3+}$. The rate constant is significantly larger than that for the proton quenching of $*Ru(bpy)_2(dpp)^{2+}$ in spite of the increased Coulombic repulsion. This suggests that quenching of $*Ru(bpy)_2(dppH_{py})^{3+}$ in this pH range is not occurring solely by diffusional processes.

In this intermediate pH range (Scheme 1), the monoprotonated complex, upon excitation, may undergo two competitive processes: A) radiative relaxation; or, B) intramolecular proton transfer from the pyridyl nitrogen to the pyrazinyl nitrogen. We postulate the latter for the following reasons: 1) NMR suggests that monoprotonation leads to twisting of the pendant pyridyl ring to allow for a hydrogen-bonding interaction with the pyrazinyl nitrogen; 2) given this cyclic structure and the significant enhanced basicity at the pyrazine nitrogen, intramolecular proton transfer would be facile within the lifetime of the monoprotonated species; and, 3) this may account for the unusually large bimolecular rate constant for protonation. Relaxation of $*Ru(bpy)_2(dppH_{pz})^{3+}$ would lead to a transfer back of the proton to reform the original monoprotonated species $Ru(bpy)_2(dppH_{py})^{3+}$.

At even higher acidities, in the low pH cycle (Scheme 1) an additional process is thought to be competitive for the excited monoprotonated complex and accounts for the further $[H^+]$ quenching from pH 2 down to pH 0: further, diffusional protonation at the pyrazinyl nitrogen to form, transiently, the diprotonated species. Any static quenching due to *ground-state, equilibrium* diprotonation might not be expected until well below $H_0 = -3$, where diprotonated complex begins to form. Excited-state protonation at the pyrazinyl nitrogen to form the diprotonated complex, whereas it is favored by the incredible increase in basicity upon population of the MLCT, would necessitate breaking the H-bonding interaction with the first proton present. Again, none of the experiments carried out during this study give any indication that the diprotonated complex, $(bpy)_2Ru(dppH_2)^{4+}$ is emissive. A bimolecular process competitive with an intramolecular process suggests that the intramolecular transfer of the proton, particularly a proton that NMR indicates is partially shared between the two peripheral nitrogens in the ground state (vide supra), must involve significant rearrangement of the surrounding water molecules. This close coupling between the proton associated with the peripheral dpp pyridine, and the solvating water molecules is thought to be the reason why protonation of peripheral pyridine dramatically increases the nonradiative rate (Table 1) even though the lack of change in the absorption spectrum points to minimal participation of the peripheral pyridine in the MLCT state. The suggestion of excited-state intramolecular proton transfer due to optically induced inversion of the relative basicities of the peripheral dpp nitrogens is similar to work done by Lay and Sasse on $Ru(bpy)_2(HOOC\text{-}bpy\text{-}COO^-)^{2+}$ where excitation leads to an inversion of basicity followed by intramolecular proton transfer.[25]

Conclusions

Population of the dpp localized MLCT state of $Ru(bpy)_2(dpp)^{2+}$ increases the basicity of the peripheral dpp nitrogens. However, ground-state protonation of the dpp peripheral pyridine, which occurs intermediate, $pK_a = 1.12 \pm 0.03$, between $[H^+]$-dependent changes evident in the emission and absorption spectra, changes the emission spectra of the complex and its subsequent protonation dynamics. Regardless of $[H^+]$, the dominant protonation process in the excited state occurs at the dpp pyrazinyl nitrogen and quenches the 705 nm emission from the dpp localized MLCT of $Ru(bpy)_2(dpp)^{2+}$. Identification of $[(bpy)_2Ru(dppH_{py})]^{3+}$ establishes that the major spectral changes originally attributed to the first protonation of $Ru(bpy)_2(dpp)^{2+}$, in fact, correspond to the second protonation and formation of $[(bpy)_2Ru(dppH_2)]^{4+}$, which is nonemissive. Instead, within the range of $[H^+]$ 10^{-2} M to 2 M, although there is little accompanying change in the absorption spectrum, the observed emission exhibits a maximum red-shifted to 735 nm and is due to that from $[(bpy)_2Ru(dppH_{py})]^{3+}$, which has an emission lifetime ≤16 ps. Protonation of the dpp peripheral pyridine dramatically increases the nonradiative rate of relaxation, but the monoprotonated complex, $[(bpy)_2Ru(dppH_{py})]^{3+}$, remains emissive, albeit weakly. The presence of the 735 nm emission from the monoprotonated complex is attributed to minimal electronic coupling of the pendent pyridine and the remainder of the dpp ligand, even though NMR indicates that the pendant pyridyl ring, initially perpendicular to the remainder of dpp ligand, twists into the plane of the coordinated pyridine and pyrazine portions of the coordinated dpp upon protonation. $[(bpy)_2Ru(dppH_{py})]^{3+}$ adopts a cyclic structure with the proton spanning both peripheral dpp nitrogens, but the proton is not equally shared being more closely associated with the dpp peripheral pyridine than with the peripheral pyrazine nitrogen. Furthermore, its presence changes the H^+ quenching dynamics from principally a diffusion limited, $k_b = 5.1 \pm 0.5 \times 10^9$ $M^{-1}\cdot s^{-1}$ bimolecular process to a combination of dynamic and static processes involving both inter- and intramolecular proton transfer between the peripheral dpp nitrogens and proton transfer from the immediate surrounding aqueous solvent shell. Förster cycle calculations suggest large increases in basicity upon excitation. However, asymmetric distribution of electron density among the different peripheral imine nitrogens affords optically induced intramolecular transfer due to an inversion of basicities in the excited state: the peripheral pyridine is more basic in the ground state, whereas the peripheral pyrazine, possessing the majority of the charge transferred on population of the dpp localized MLCT state, is more basic in the excited state. Thus, it is critical to be cognizant of multiple protonations sites in close proximity when calculating optically induced changes in

acid−base behavior. The implications of an inversion in basicity between the two peripheral imine nitrogens on coordination in the ground and excited states will be examined in future articles.

Acknowledgment. H.D.G. gratefully acknowledges support of this research by the National Science Foundation (CHE-0079040 and CHE-0514458), the Petroleum Research Foundation administered by the American Chemical Society, The City University of New York Center of Advanced Technology in Photonics designated by the New York State Science and Technology Foundation, and the CUNY PSC-BHE Grants Program. J.L.Z. gratefully acknowledges the National Science Foundation for a Graduate Research Fellowship, and a GK-12 Fellowship. J.L.Z. also acknowledges the CUNY Louis Stokes Alliance for Minority Participation for several Graduate Assistantships, and Dissertation Fellowship. E.X.F. thanks the City University of New York Doctoral Program in Chemistry for a Graduate Research Award. We also thank Professor Robert Alfano and Dr. Bidyut Das of the CUNY Institute for Ultrafast Spectroscopy and Lasers for the picosecond measurements.

Supporting Information Available: Proton NMR of the titration of $Ru(bpy)_2(dpp)^{2+}$ with D_2SO_4 showing the downfield shifts of specific dpp protons with increasing acid concentration; plot of the relative quantum yields (Φ/Φ_o) and relative emission lifetimes (τ/τ_o) of the 705 nm emission of $Ru(bpy)_2(dpp)^{2+}$ vs pH; plots and sigmoidal fits of contributions of the 705 nm (◊) and 735 nm (□) emissions to the composite emission spectra in the acid titration of $Ru(bpy)_2(dpp)^{2+}$. The fits inflect and cross at pH 3.1. This material is available free of charge via the Internet at http://pubs.acs.org.

References and Notes

(1) Hicks, C.; Ye, G.; Levi, C.; Gonzales, M.; Rutenberg, I.; Fan, J.; Helmy, R.; Kassis, A.; Gafney, H. D. *Coord. Chem. Rev.* **2001**, *211*, 207–222.

(2) Kalyanasundaram, K. *Coord. Chem. Rev.* **1982**, *46*, 159–244.

(3) Banks, C. V.; Bystroff, R. I. *J. Am. Chem. Soc.* **1959**, *81*, 6153–6158.

(4) Dougherty, T.; Hicks, C.; Maletta, A.; Fan, J.; Rutenberg, I.; Gafney, H. D. *J. Am. Chem. Soc.* **1998**, *120*, 4226–4227.

(5) Peterson, S. H.; Demas, J. N. *J. Am. Chem. Soc.* **1976**, *98*, 7880–7881.

(6) Fan, J.; Helmy, R.; Kassis, A.; Grunseich, A.; Mangubat, P.; Hicks, C.; Stevens, N.; Gafney, H. D. *Inorg. Chem.* **2003**, *42*, 2486–2488.

(7) Shimidzu, T.; Iyoda, T.; Izaki, K. *J. Phys. Chem.* **1985**, *89*, 642–645.

(8) Hosek, W.; Tysoe, S. A.; Gafney, H. D.; Baker, A. D.; Strekas, T. C. *Inorg. Chem.* **1989**, *28*, 1228–1231.

(9) Nazeeruddin, M. K.; Kalyanasundaram, K. *Inorg. Chem.* **1989**, *28*, 4251–4259.

(10) Braunstein, C. H.; Baker, A. D.; Strekas, T. C.; Gafney, H. D. *Inorg. Chem.* **1984**, *23*, 857–864.

(11) Williams, A. T. R.; Wenfield, S. A.; Miller, J. N. *Analyst* **1983**, *108*, 1067–1071.

(12) Pranzo, P. Princeton Instruments, personal communication, 2009.

(13) Ferrari, M. B.; Fava, G. G.; Pelssi, G.; Predieri, G.; Vignali, C.; Denti, G.; Serroni, S. *Inorg. Chim. Acta* **1998**, *275−276*, 320–326.

(14) Cook, P. F. *Enzyme Mechanism from Isotope Effects*; CRC Press: Boca Raton, FL, 1991.

(15) Zambrana, J. L., Jr.; Ferloni, E. X.; Colis, J. C.; Gafney, H. D. *Inorg. Chem.* **2008**, *47*, 2–4.

(16) Hoffman, M. Z.; Bolleta, F.; Moggi, L.; Hug, G. L. *J. Phys. Chem. Ref. Data* **1989**, *18*, 219–543.

(17) Ireland, J. F.; Wyatt, P. A. H. *Adv. Phys. Org. Chem.* **1976**, *12*, 131–221.

(18) Van Houten, J.; Watts, R. J. *J. Am. Chem. Soc.* **1976**, *98*, 4853–4858. Nakamaru, K. *Bull. Chem. Soc. Jpn.* **1982**, *55*, 2697. Johansen, O.; Launikonis, A.; Mau, A. W. H.; Sasse, W. H. F. *Aust. J. Chem.* **1980**, *33*, 1643. McClanahan, S. F.; Dallinger, R. F.; Holler, F. J.; Kincaid, J. R. *J. Am. Chem. Soc.* **1985**, *107*, 4853.

(19) Zambrana, J. L., Jr. In *Chemistry Doctoral Program*; City University of New York: New York City, 2007; p 339.

(20) Lipkowski, J. *Cryst. Struct. Comm.* **1976**, *5*, 931–934.

(21) Su, H.; Kincaid, J. R. *JRS* **2003**, *34*, 907–916.

(22) Förster, T. *Z. Electrochem.* **1950**, *54*, 531.

(23) Ferloni, E. X.; Gafney, H. D. ACS National Meeting; Boston, MA, 2007.

(24) Rugge, A.; Clark, C. D.; Hoffman, M. Z.; Rillema, D. P. *Inorg. Chim. Acta* **1998**, *279*, 200–205.

(25) Lay, P. A.; Sasse, W. H. F. *Inorg. Chem.* **1984**, *23*, 4123–4125.

JP903521P